Title: Interface Resolved Simulations of Reactor Flows

Authors: Jun Fang[a], Joseph J. Cambareri[b], Mengnan Li[b], Nadish Saini[b], Igor A. Bolotnov[b*]

Affiliations:

[a] Argonne Leadership Computing Facility, Argonne National Laboratory, Lemont, IL 60439

[b] Department of Nuclear Engineering, North Carolina State University, Raleigh, NC 27695

Email: *igor_bolotnov@ncsu.edu (I.A. Bolotnov)

Author proof:

Prof. Igor A. Bolotnov

(518) 542-8939

igor_bolotnov@ncsu.edu

Campus Box 7909

3140 Burlington Engineering Labs

2500 Stinson Drive

Raleigh, NC, USA 27695-7909

Manuscript total number of pages: 40

Table list:

Figure list:

Interface Resolved Simulations of Reactor Flows

Jun Fang[a], Joseph J. Cambareri[b], Mengnan Li[b], Nadish Saini[b], Igor A. Bolotnov[b*]

[a] Argonne Leadership Computing Facility, Argonne National Laboratory, Lemont, IL 60439

[b] Department of Nuclear Engineering, North Carolina State University, Raleigh, NC 27695

*igor_bolotnov@ncsu.edu (I.A. Bolotnov)

ABSTRACT

The presented review paper outlines the recent progress in high-resolution numerical simulations of two-phase coolant flow in LWR relevant geometries by resolving the water-vapor interface. Rapid development of high-performance computing capabilities is creating exciting opportunities to study complex reactor thermal hydraulic phenomena. Today's advances in thermal hydraulic analysis and interface resolved simulations will help pave the way to the next level of understanding of two-phase flow behavior in complex geometries. This paper consists of two major parts: (i) a brief review of direct numerical simulation and interface tracking simulation, and (ii) several opportunities in the near future to apply cutting-edge simulation and analysis capabilities to address the nuclear related multiphase flow challenges. The first part will discuss typical computational methods used for those simulations, provide some examples of the past work, as well as computational cost estimates and affordability of such simulations for research and industrial applications. In the second part specific application examples are discussed, from adiabatic bubbly flow simulations in PWR subchannel geometry to the modeling of nucleate boiling. The uniqueness of this study lies in the specific focus on applications with nuclear

engineering interest as well as new generation modeling and analysis methodologies. Together with the ever-growing computing power, the related large-scale two-phase flow simulations will become indispensable for the improved scientific understanding of complex two-phase flow phenomena in nuclear reactors under normal operation and postulated accident conditions.

KEYWORDS

Two-phase flow, direct numerical simulation, interface tracking, subchannel geometry

I. INTRODUCTION

Fluid flow and turbulence is one of the complex physical phenomena which cannot be typically described using simple analytic solutions. In the early days of nuclear thermal hydraulics, the most common approach was to develop experimentally-based empirical correlations for one-dimensional flow models. Those correlations are typically limited for specific flow geometry and are valid for specific range of flow parameters.

Somewhat more universal modeling approach involves three-dimensional representation of the flow domain and being referred to as computational fluid dynamics (CFD). It does require quite significant computational resources, and thus only recently reach nuclear engineering community as a practical tool to assist in design and modeling of reactor-relevant flows. The traditional CFD does require modeling closures, and thus also has its own practical limits. The basic set of turbulence models used in research and commercial flow simulation codes has been developed in the 1970s[1–3] for single-phase flows and modified for two-phase flows in the 1990s[4]. The new century brought us advanced computing capabilities[5] and advanced numerical methods[6] to allow for major improvements in the way we model two-phase flow: (i) modeling approach now can be more computationally expensive by applying higher resolution models; (ii) the development and validation can be enhanced by means of affordable direct numerical simulation (DNS) which can provide great insight into complex flow structures.[7–12]

Turbulence modeling approaches typically utilize the Reynolds-averaged Navier-Stokes (RANS) equations[13] which assume that the flow velocity field can be split into the mean and fluctuating components. The mass and momentum equations are solved for the mean quantities and closure laws for so-called Reynolds stress tensor are required to represent the effect of the unresolved fluctuations on the mean velocity field. Many models[14] use the Boussinesq

approximation[15] by introducing the turbulent viscosity, ν_T, to model the turbulence. Averaging of the Navier-Stokes equations (NSE) allows solving them on much coarser grids compared to the length scale of turbulent fluctuations.[16]

In contrast to single-phase turbulence, much less research has been done for turbulent two-phase flows. Two-phase turbulence simulation and analysis play a pivotal role in many engineering disciplines, including nuclear, chemical and biomedical engineering[6], because good two-phase turbulence models are needed to accurately predict phase distribution phenomenon. Specifically, in nuclear engineering, a reliable prediction of phase distribution is crucial in nuclear safety analysis since it has a direct impact on the efficiency of heat transfer and neutron moderation. Meanwhile, the modeling of two-phase turbulence is even more complicated and requires a larger amount of closure laws in RANS framework to predict the flow behavior.[4,6,17,18] The need of these closures arises from the derivation of two-phase flow RANS equations from first principles.[19]

Unlike the RANS-based models, DNS approach directly solves the NSE. This approach relies on full three-dimensional, space and time resolved simulations with strict grid resolution requirements. It is a relatively new direction in turbulence studies since it has become affordable only in the past three decades for meaningful applications. Early research performed the simulations of single-phase turbulent flow in a flat channel at relatively low Reynolds numbers[20] (about 180 based on friction velocity and channel half-width). The development of high-performance computing (HPC) allowed the increase of the resolved friction Reynolds numbers up to 5200.[10,21] DNS has been also used to study the effect of wall roughness on the flow.[9,22,23] In addition, the channel flow DNS provided much better understanding of turbulence and led to the development of new turbulence models[24,25] based on the analysis of the DNS database[7].

Direct numerical simulation of turbulent flows has been coupled with interface tracking methods (ITM) to extend the simulation capability to two-phase flows. Mainstream interface tracking methods include volume of fluid (VOF)[26], front-tracking method[27] and level-set methods[28]. In the past decade, DNS and interface tracking has been widely used to study bubble-turbulence interaction. Ilic et al. quantified the turbulent kinetic energy balance in bubble induced turbulence[29] and evaluated the energy spectra in bubble driven liquid flows using DNS[30]. Note that in this scenario the bubble-induced turbulence was not superimposed on the existing single-phase turbulence (as it typically happens in boiling flow simulations). Turbulent bubbly channel flows were extensively studied by Tryggvason et al.[8,12,31] using the front tracking method. The related DNS investigations have revealed that the bubble deformation strongly affects the interfacial forces (e.g. drag or lift), hence resulting in very different void fraction profiles depending on the Eötvös number. Based on the DNS database of two-phase flow in vertical channels, Bois[32] and du Cluzeau et al.[33] proposed improved transport equations of Reynolds stress by accounting for the interfacial contributions. Bolotnov et al.[34] investigated the turbulent bubbly channel flow using the level-set method approach and later performed turbulence anisotropy analysis for bubbly turbulence with Reynolds number up to 400 (based on friction velocity)[11]. The related progresses and challenges encountered are periodically reviewed by various authors. For examples, Tryggvason et al.[12] reviewed the ITM progress and pointed out the pressing needs to develop new models for large-scale, or average multiphase flows based on the input and insights from DNS results. More recently, Elghobashi presented a comprehensive review on the DNS of turbulent flows laden with droplets or bubbles.[35] The available literature was categorized there into two major groups based on the dispersed entity size with respect to the Kolmogorov length scale. Conventionally, the interface resolved simulations were limited to either low Reynolds numbers

and only tens of bubbles[27,34] or simplified geometries like a flat channel, and thus could produce limited information about real-world bubble/liquid interactions in complex engineering systems.

The latest advances in numerical methods and HPC facilities now enable researchers to apply the interface resolved DNS into problems with direct nuclear engineering interest. Most recently, Fang et al. conducted several studies of single- and two-phase flows in nuclear reactor subchannels[36,37] as well as fully resolved two-phase flow simulations for subchannels with mixing vanes and spacer grids[38,39]. The related simulations not only consider the fluid properties of water and vapor under reactor operation conditions, but also adopt realistic subchannel structures in the computational domains. Moreover, the bubble evaporation/condensation and boiling modeling is also being actively pursued[40–43] and will be incorporated in future interface resolved DNS to give a complete representation of reactor two-phase coolant flow conditions. Figure 1 clearly demonstrates the tremendous growth of single- and two-phase DNS modeling both in capabilities and engineering relevance over the past several decades, as discussed in Fang et al.[38] As one can observe, we are currently at the tipping point of simulation capabilities when nuclear reactor flows can be fully resolved with modern computing methods and facilities, and focus should be placed on model development based on validated high resolution simulations. In the presented manuscript we are focusing on the work building up on this experience and discuss the path forward for the interface tracking analysis contribution for the advanced thermal hydraulics research area.

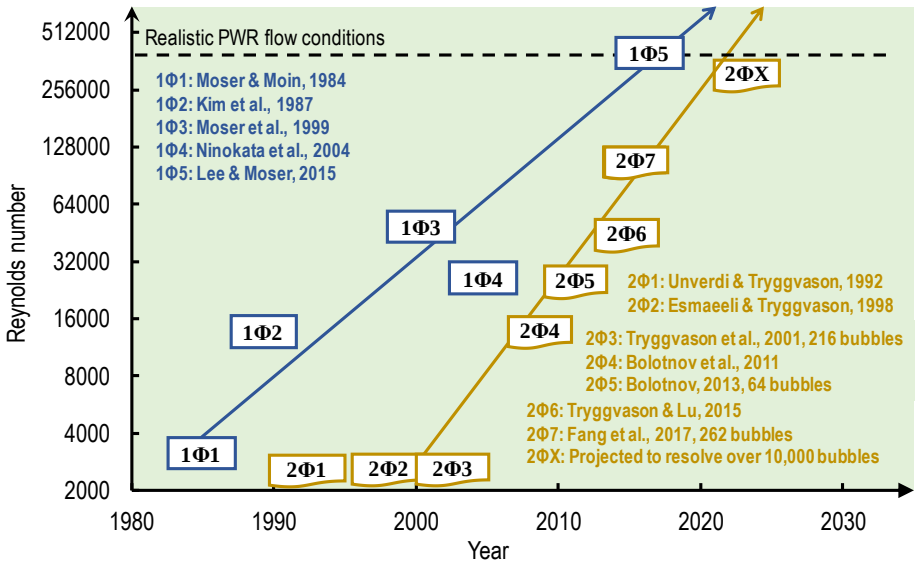

Figure 1. DNS capabilities evolution for single (1Φ) and two-phase (2Φ) flows over the years as outlined in Fang et al.[38]

II. METHODOLOGY

The presented research results utilize power research DNS code, PHASTA. This is a three-dimensional finite element method (FEM) flow solver for both incompressible and compressible flows. The level-set method was implemented in PHASTA to simulate various two-phase flows[44]. Recently, a bubble tracking method has been added to PHASTA to collect detailed bubble parameters as the simulation progresses.[37] Since it's based on FEM formulation, the code readily supports unstructured grids, which makes it suitable for simulation of turbulent flows in complex engineering geometries, such as the PWR fuel subchannel with spacer grids and mixing vanes[39]. Highly scalable performance (up to 768×1024 processing cores) on massively parallel computers has been demonstrated with PHASTA on several top-ranked supercomputers[45]; PHASTA is a proven tool for large scale simulation of turbulent two-phase flows.

II.A. Governing equations

Transient incompressible Navier-Stokes (INS) equations are solved in three dimensions using a stabilized finite element method (FEM).[46] The discretization details used in the PHASTA code have been discussed in Nagrath et al.[44] Mass and momentum conservation for incompressible flows can be written as:

$$\frac{\partial u_i}{\partial x_i} = 0 \tag{1}$$

$$\rho \frac{\partial u_i}{\partial t} + \rho u_j \frac{\partial u_i}{\partial x_j} = -\frac{\partial p}{\partial x_i} + \frac{\partial \tau_{ij}}{\partial x_j} + f_i \tag{2}$$

where u_i is the velocity in the *i*-th dimension (i = 1, 2 and 3), ρ denotes the density of the fluid, p the static pressure and τ_{ij} the viscous stress tensor. f_i represents the *i*-th component of the body force vector. For the incompressible flow of Newtonian fluid, the viscous stress tensor is related to the fluid viscosity μ and the strain rate tensor, S_{ij}, as:

$$\tau_{ij} = 2\mu S_{ij} = \mu(\frac{\partial u_i}{\partial x_j} + \frac{\partial u_j}{\partial x_i}) \tag{3}$$

Continuum Surface Force (CSF) model proposed by Brackbill et al.[47] is utilized to represent the surface tension force as a local volumetric force density across the interface region (included in f_i).

II.B. Level set method

The level-set method has been used as one of the major interface tracking approaches in multiphase flow simulations. This method has been developed by Sussman et al.[28], and has been implemented in PHASTA to extend the simulation capability from single-phase to two-phase flows[44]. It has been demonstrated that the level set method is capable in simulating various two-

phase flow regimes, including bubbly flow[34], slug flow[48], slug-churn[49] and even annular flow[50]. The interface is represented as the zero-level set of a smooth function, φ. This function represents the signed distance from the interface. The scalar, φ, is advected with the fluid according to the advection:

$$\frac{D\varphi}{Dt} = \frac{\partial \varphi}{\partial t} + \boldsymbol{u} \cdot \nabla \varphi = 0 \tag{4}$$

The gas phase is indicated by a negative level set, $\varphi < 0$, while the liquid phase by the positive, $\varphi > 0$.

Since for fixed meshes it is quite challenging to represent the jump in fluid properties across the interface, a finite interface thickness is assumed, and the properties over the interface are approximated using a smoothed Heaviside function:

$$H_\varepsilon(\varphi) = \begin{cases} 0 & \text{for } \varphi < -\varepsilon \\ \frac{1}{2}\left[1 + \frac{\varphi}{\varepsilon} + \frac{1}{\pi}\sin\left(\frac{\pi\varphi}{\varepsilon}\right)\right] & \text{for } |\varphi| < \varepsilon \\ 1 & \text{for } \varphi > \varepsilon \end{cases} \tag{5}$$

The true distance field will be stretched by the non-zero local velocity gradient, so the level set field is corrected at every time step with a re-distancing operation. More details on the advection and re-distancing processes has been documented before[28,34].

II.C. Bubble tracking method

While level set has been proven to work well to track the interface, in complex two-phase flow simulations collecting statistics for individual entities (bubbles or droplets) is an invaluable ability for model development. Following individual bubbles allows to evaluate the flow information, such as bubble velocity, volume, deformation level, and even the local liquid velocity and shear rate as a function of time for each bubble or droplet. This method has been introduced by Fang et al.[37] The basic idea is to introduce a bubble indicator field which is advected to

dynamically mark and track each of the simulated bubbles or droplets. Associated data extraction techniques are developed in Fang et al.[37] to record the important parameters of bubble behavior and local fluid conditions. We will provide a few new examples in this paper about how this approach benefits the understanding of the complex two-phase flows.

II.D. ITM Boiling Model

An ITM based boiling model has recently been developed and implemented in PHASTA to enable large scale boiling simulations in complex geometries[51]. The phase-change process is governed by an evaporation-condensation model[52], which couples a scalar equation that calculates the gas volume increase/decrease due to local interface temperature gradient with the continuity and momentum equations. A saturation temperature is assumed for vapor bubbles. The temperature field is solved over the course of simulations. The local temperature gradient is estimated to obtain the averaged heat flux through the interface according to the temperature distribution around each bubble. The volume change based on average heat flux is added into the mass conservation equation as a volumetric source term controlling the growth rate. This approach ignores the effect of local temperature variance on the bubble growth. In exchange, the averaging makes the simulations more stable and allows for smooth bubble growth and condensation even during possible localized temperature fluctuations.

The evaporation-condensation model is coupled with the aforementioned *Bubble Tracking Method* (BTM) to achieve multiple bubble evaporation/condensation. BTM introduces an additional bubble ID field to identify and track each individual bubble in the domain. The nodes within the region of interest are colored by the corresponding bubble ID while the rest of the domain is marked by the zero ID value. The region of interest consists of two parts: the bubble region (to collect the bubble-related information) and a near interface liquid shell (to collect local

liquid information). The temperature gradient information is collected from the "liquid shell" region. After coupling with BTM, the evaporation-condensation model can estimate the average temperature value for every bubble and achieve different growth rate for each bubble at various heat transfer conditions. Part of the verification results of this model has been presented by Li and Bolotnov[53].

The wall effect is considered through a contact angle control model. The contact angle plays an essential role in determining the characteristics of boiling phenomena like nucleation site density, bubble departure diameter, and bubble release frequency. The value of contact angle is influenced by the solid surface, liquid and vapor properties at micrometer-scale and nanometer-scale, which is beyond the resolvable scale range in interface tracking simulations. To properly account for the contact angle effect, a contact angle control model is developed at millimeter-scale (the scale length of interface tracking simulations) and implemented as a sub-grid force model in PHASTA[54]. The influence of surface effects on contact angle is represented by the value of prescribed target contact angle in the algorithm. The control force is applied when the current contact angle deviates from the desired value (or range of values) and decrease to zero when the current contact angle reaches the desired value. The advancing and receding contact angles are treated separately in consideration of the lateral movement of the bubble.

The microlayer evaporation is not considered in the current boiling framework yet. It is known that vapor generated via microlayer evaporation is an important contributor to the early stage of bubble growth in low-pressure boiling, but there is still no consensus regarding the mechanism of microlayer evaporation. Varying contributions of microlayer evaporation to bubble volumetric growth in boiling were reported by different researchers, and this value could be 60% according to Sato and Niceno[55] or around 20% suggested by Kim and Jungho[56]. The ITM boiling model in

PHASTA is designed to enable phase-change in large scale simulation with thousands of bubbles and investigate the bubble dynamics under complex flow conditions. The micro-layer evaporation, compared to the turbulence effect, bubble-bubble interactions, flow-structure interaction, etc., is not among the current priorities, but left for future improvement.

II.E. DNS mesh design

The major computational expense in performing DNS comes from strict computational mesh resolution requirements. For two-phase flows the issue complicates due to interface curvature / bubble size mesh requirements. To ensure an accurate representation of relevant turbulent scales and bubble behavior in the simulations the following conditions must be met: (1) the computational domain must be sufficiently large to contain the largest turbulent eddies; (2) the mesh cell size must be sufficiently small to resolve the small scales of interest in liquid turbulence; (3) the resolution of bubble interface and the vicinity regions should be fine enough to properly capture the interface topology changes as well as the eddies in the wake flow behind a bubble. The periodic inlet/outlet condition is typically adopted to allow the proper resolution of the large turbulent eddies in the flow. To meet the second prerequisite, the mesh cell sizes should be comparable to the local Kolmogorov length scale. Since the calculation of the Kolmogorov scale requires values of the turbulence dissipation rate, which are not known a priori, several scoping runs are typically performed to get the approximated Kolmogorov length scales. The computational mesh would be refined if the existing mesh cell size is much larger than the Kolmogorov scale. The third requirement has been evaluated in the previous meshing studies and it was revealed that an minimum resolution of 20 mesh cells across the bubble diameter is adequate to properly capture the bubble behavior in our level set based two-phase flow simulations.[34]

III. APPLICATIONS

This section briefly reviews the application examples leveraging high-resolution interface tracking simulations to study various two-phase reactor flow problems: (i) adiabatic bubbly flow in PWR subchannels, (ii) multiple bubble flow boiling simulation and (iii) adiabatic modeling of droplet/spacer grid interaction analysis during dispersed flow film boiling regime (DFFB). These flow problems are highly relevant to either reactor normal operation or accident scenarios, of which the experimental investigations are very difficult or costly to perform. The validated high-resolution numerical simulations can offer valuable complementary insights in a cost-efficient way.

III.A. Reactor geometry bubbly flow simulations

To maintain the core structure and achieve high heat removal efficiency, the nuclear fuel rods are commonly arranged together in a triangle or square pattern with spacer grids. Mixing vanes are installed on some of the spacer grids to promote the turbulence intensity, and thus the convective heat transfer rate. The entire coolant passage can be regarded as a collection of the individual conduits bounded by neighboring fuel rods, and such individual conduit is referred as the subchannel here. Reactor core geometry two-phase flow simulations focus on single subchannel simulations of bubbly flow. As shown in Figure 2, the computational domain consists of a subchannel together with spacer grid and mixing vanes to study the effects of these complex geometries upon the flow. The discretization of computational domain results in 2.5 billion mesh cells. Periodic boundary condition is applied to the domain inlet and outlet as well the transverse faces, while no-slip condition to the surfaces of fuel rod, spacer grid and mixing vanes. Due to the strict CFL constraints in two-phase flow simulations and huge amount of mesh entities, it is

estimated to consume 47.13 million CPU-hours to achieve one flow-through.[1] To minimize the computational cost, single-phase turbulence is first simulated in the same geometry to the quasi steady-state, and then bubbles are introduced in the flow for the subsequent runs. The simulations were carried out on the BlueGene/Q machine, Mira, at Argonne National laboratory. Table 1 lists the primary geometric and flow properties that were applied in the current investigation.

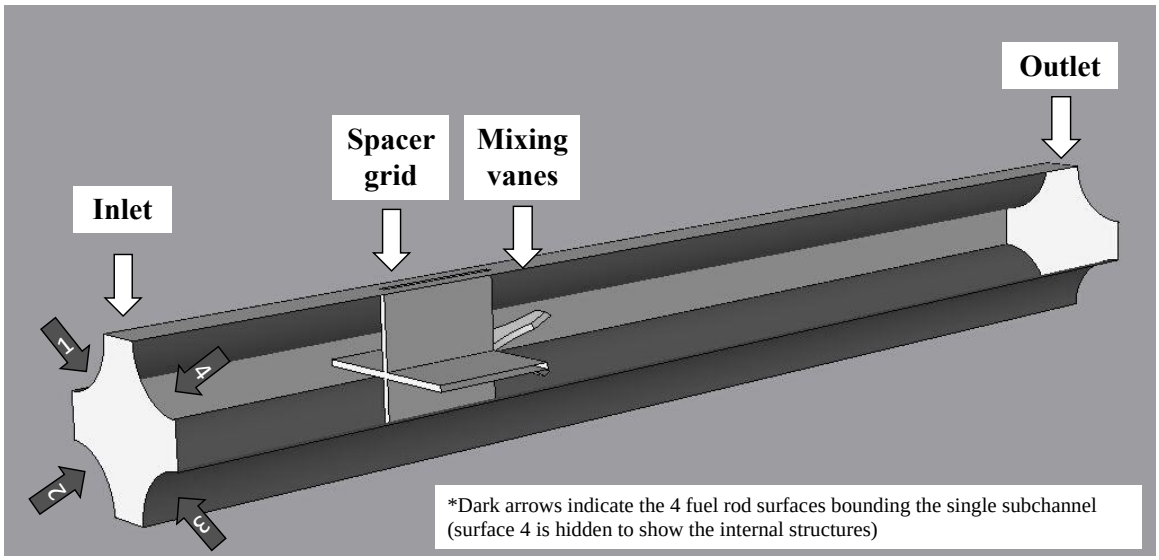

Figure 2. The sketch of the computational domain of a single PWR subchannel.

Table 1. Computational parameters in subchannel bubbly flow simulation.

Parameter	Value
Fuel Rod Radius (*mm*)	4.57
Domain Height (*mm*)	100
Bulk Mesh Size (μm)	29.30
Total Number of Mesh Elements	2.50 billion
Number of Resolved Bubbles	655
Resolved Bubble Diameter (*mm*)	0.6509
Mean Axial Velocity (*m/s*)	0.75
Hydraulic Reynolds Number (Re_h)	80,000

[1] The Computational cost is estimated on the BG/Q Mira HPC at Argonne National Laboratory.

To make best use of these expensive simulations, the bubble tracking algorithm is employed to record the complete evolution history of bubbles' dynamics over the course of simulations (shown in Figure 3).

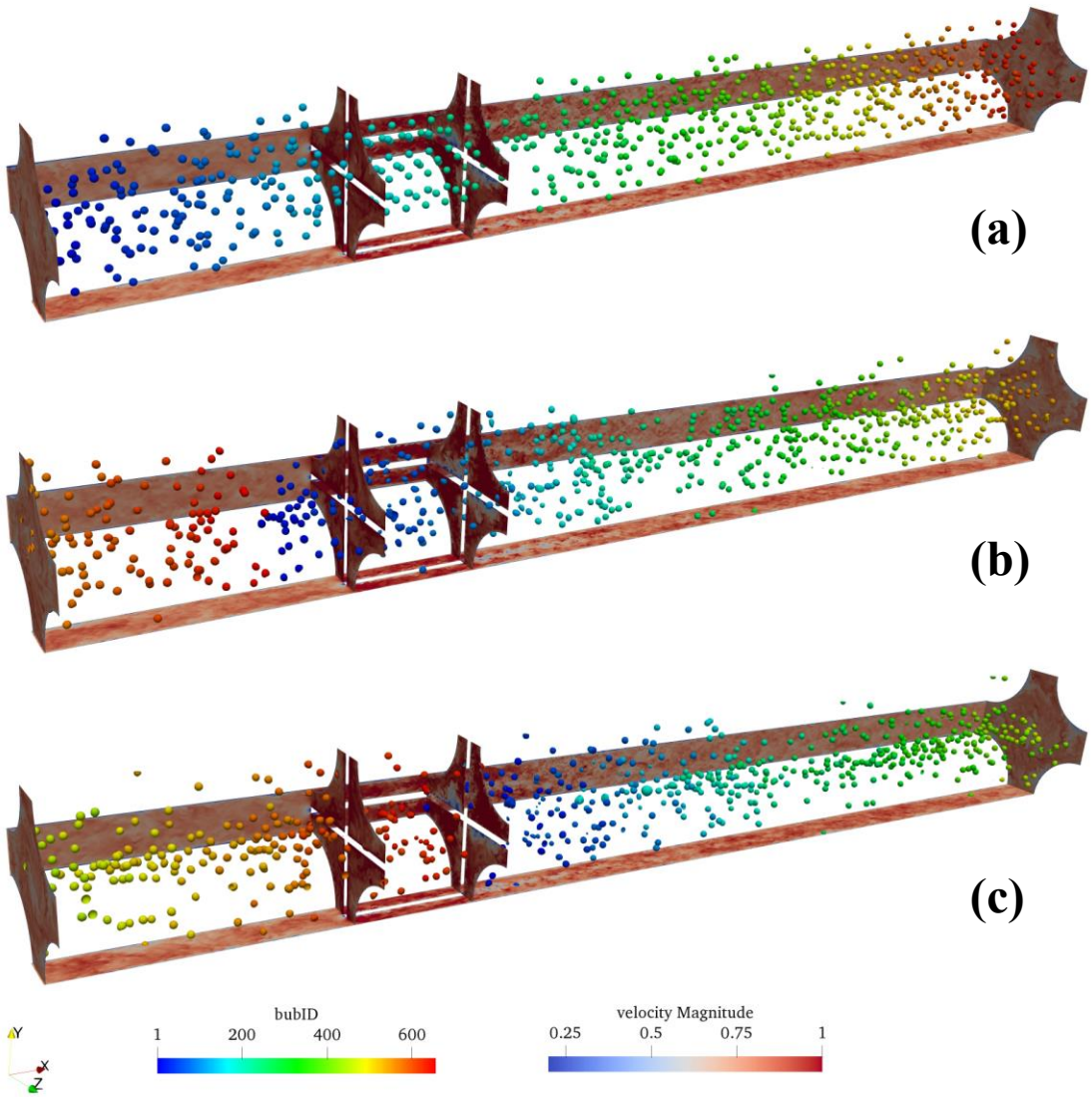

Figure 3. DNS simulation of 655 bubbles traveling through nuclear subchannel with spacer grids/mixing vanes.

With the abundant numerical information concerning bubble behavior in the reactor subchannel geometry, the development of advanced statistical analysis tools is necessary to process it. One example of such analyses is the group averaging, which divides the entire bubble

population into subgroups based on the bubble's distance from the nearest fuel rod surface. Here, the centrifugal effect induced by the spacer grids and mixing vanes upon the void fraction distribution can be observed within the subchannel domain (as shown in Figure 4). Typically, pipe flow simulations observe a wall peaked void fraction profile. However, with the inclusion of the mixing vanes, the swirling effect promotes bubble migration towards the center of the channel, resulting in a center peaked profile. The group averaged bubble drag coefficient also exhibits significant dependency on wall distance, indicating the conventional drag model lacking wall distance dependence may be inadequate in representing the underlying physics. The strong swirling effect that exists downstream from the spacer grid and mixing vanes region is exhibited to have a large impact on the reported bubble drag coefficient and deformability (Figure 5 and Figure 6). However, this effect decays when the flow moves further downstream. As bubbles enter the mixing vane region, they observe a large increase in their reported drag coefficient, associated with the bubbles becoming less deformed. The deformability factor is defined with a range from 0 to 1, and in such a way that a perfectly spherical bubble is reported to have a value of 1 and the bubble is deemed more deformed when the factor is closer to 0.[37] The impact of spacer grid and mixing vanes on average drag coefficient and bubble deformability almost vanishes in 3 to 4 mixing vane heights. More details are documented in Fang et al.[39] Advanced analysis of this kind can hopefully shed light into the physics underneath the bubbly flow and facilitate the development of more accurate closure laws.

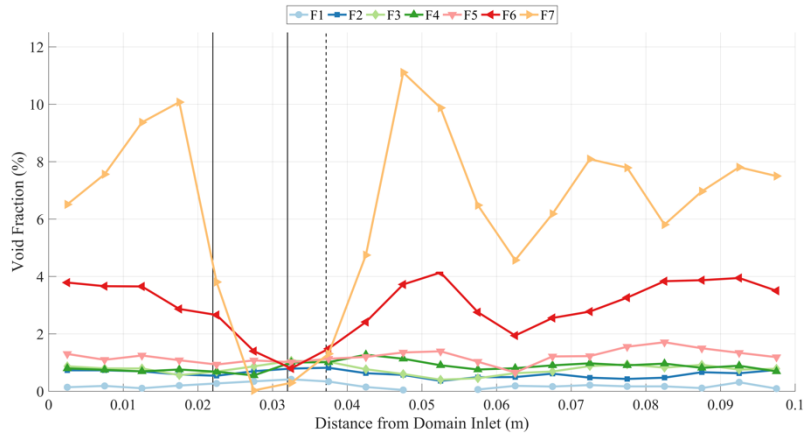

Figure 4. Evolution in the void fraction for each distance to the fuel rod surface group as a function of the distance from the domain inlet.

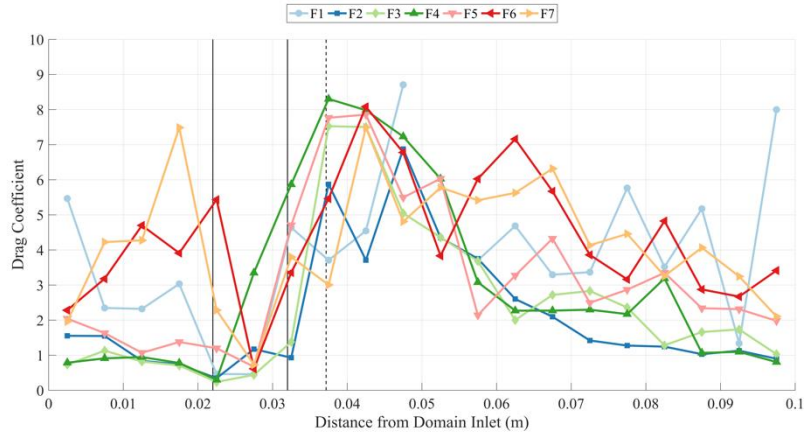

Figure 5. Change in the reported bubble drag coefficient in each distance to the fuel rod surface group as a function of the distance from the domain inlet.

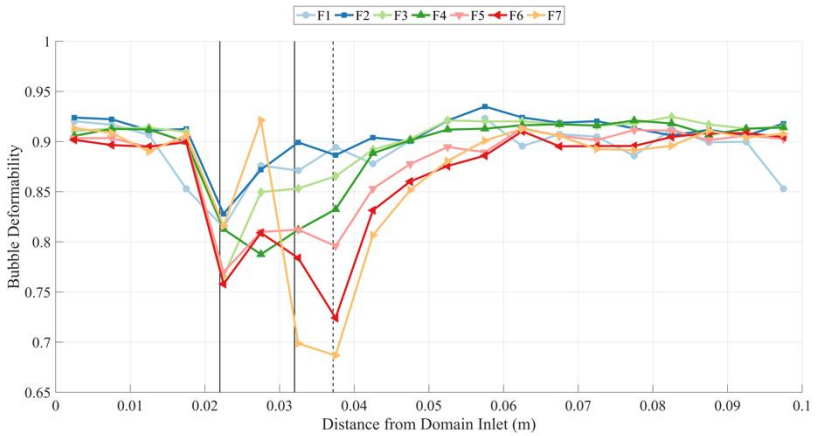

Figure 6. Distribution of the bubble deformability for each distance to the fuel rod surface group as a function of the distance from the domain inlet.

III.B. Multiple bubble boiling simulations

To develop the modeling capability of boiling phenomenon in the PHASTA code, the dedicated efforts started with the coupling and verification of the energy equation solver and the volume generation term to solve the bubble evaporation problem[53]. A following step was to evaluate the pool boiling behavior using the previously implemented contact angle control algorithm.[54,57] The current numerical investigation examines the behavior of multiple bubbles under more complex thermal and hydrodynamic conditions. Four bubbles are initialized on the heated walls with a deflected plate structure in the domain center, resembling a simplified spacer grid and mixing vane (Figure 7) and providing time varying flow conditions at the bubble nucleation site. This plate consists of a main part parallel to the walls along with a deflected tail. The existence of this structure can disturb the main flow stream and induce turbulence in the wake region. The vortices generated also enhance the temperature mixing and the heat transfer rate downstream the plate. This entire design serves as an approximated representation of the realistic flow conditions near mixing vanes in the PWR core. The computational domain is outlined in Figure 7. A periodic boundary condition is applied to the side walls. Uniform inflow is applied to the inlet face while the natural pressure for the outlet. A constant heat flux boundary condition $q'' = 180\text{kW/m}^2$ is applied to the heated patch on the bottom wall. The inflow is subcooled with a temperature of $92℃$. The thermal properties used in the simulation are listed in Table 2. The final mesh is of about 9.6 million unstructured elements, and the production runs are carried out on 256 parallel cores.

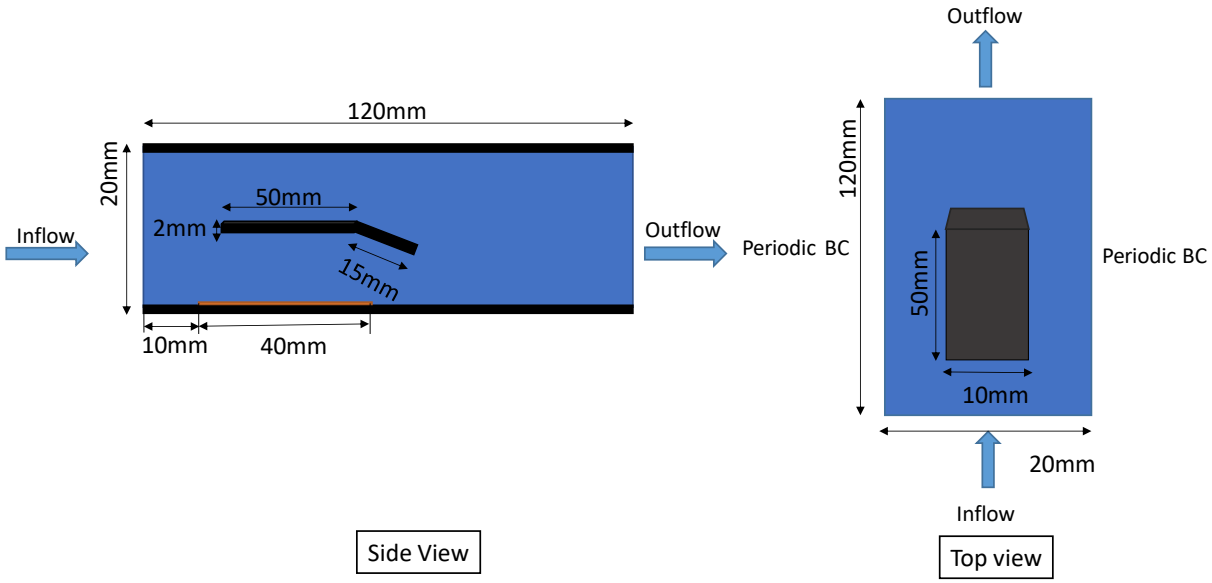

Figure 7. The schematic picture of the domain design.

Prior to the introduction of bubbles, the single-phase flow simulation is performed first. The deflected plate invokes flow instabilities, and results in a significant velocity increase in the region near the inclined tail. The presence of the plate also insulates the heated wall from the top wall region (Figure 8). Four nucleation sites are selected in the domain to initialize bubbles with different local hydrodynamic and thermal conditions. Local grid refinement is applied around the nucleation sites to better resolve the bubble shape as well as the sharp temperature gradients across the bubble interface accurately. The boundary layer mesh is adopted in the near wall region for an accurate estimation of the local contact angle and proper boundary layer development. The influence of local environment on bubble behavior is to be studied. As shown in Figure 8, the first bubble site is placed near the subcooled inlet flow, bubble condensation is expected to occur here according to the obtained temperature distribution. The second and the third bubble are under the simulated spacer grid. The superheat rate is relatively high in this region. The heat accumulates along the channel as the flow develops, so the third bubble is anticipated to have a higher

evaporation rate compared with the second bubble and depart earlier due to the high local velocity. A slow departure of the fourth bubble is expected due to the smaller local drag and lift force on the growing bubble.

Table 2. The fluid properties in the multi-bubble flow boiling simulation.

Parameters	**Water**	**Vapor**
Density kg/m^3	958.0	0.579
Thermal conductivity $W/(m \cdot ℃)$	0.679	0.025
Specific heat $kJ/(kg \cdot ℃)$	2.80	2.034
Saturation temperature ℃	100	
Latent heat kJ/kg	2260.0	

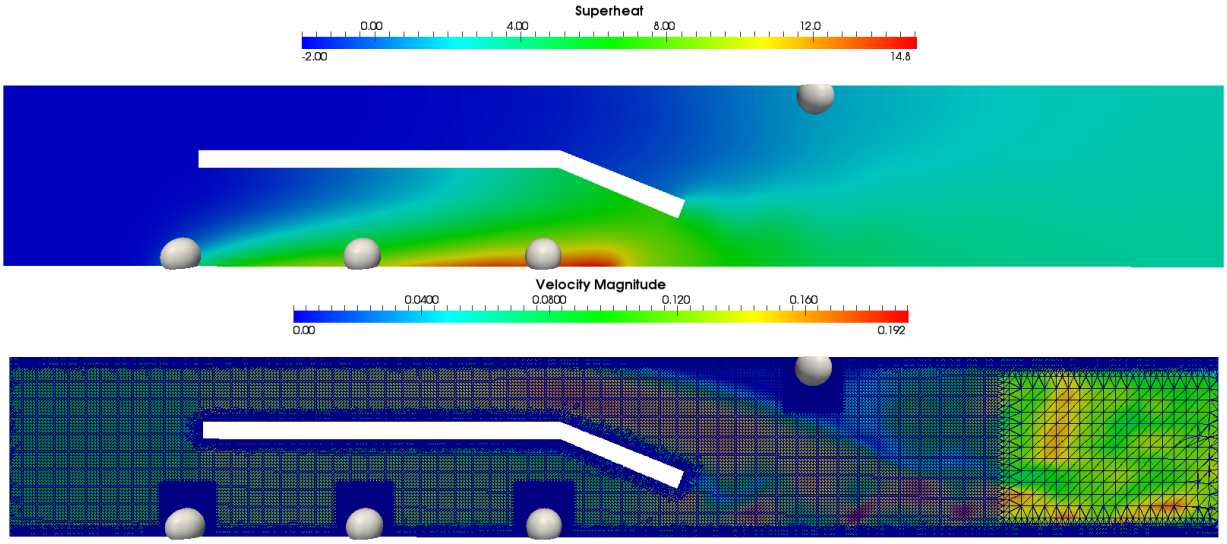

Figure 8. The initial bubble positions in the domain. The temperature field is shown on the top picture while the velocity field is shown on the bottom with the mesh design in the background.

The snapshots in Figure 9 show the bubbles' growth and departure during the flow boiling. The evolution of the local contact line (the triple contact line between solid, liquid and gas phase) indicates the movement of the interface due to the application of contact angle control algorithm. The local superheat/subcooling results in various temperature gradients around each bubble. The first bubble departs earliest from the wall ($t = 1.83ms$) and it's followed by the second bubble ($t = 2.11ms$). The third bubble lift off from the wall at around $2.62ms$, and the forth bubble is slightly later. The bubble tracking analysis (BTA) is utilized in the multiple bubble flow boiling

simulation to collect the history information of individual bubbles. The evolution of bubble radius over time is presented in Figure 10. After the departure from the wall, the first bubble is observed to condense after 5ms due to the increasing local subcooled condition created by the inlet flow. The volume of the second bubble keeps increasing from the beginning to about 12 *ms*, and decreases when the bubble moves upward to the subcooled region. The third bubble sees the largest volume growth. It reaches the maximum volume at around $14\,ms$, and then condenses when entering the subcooled region. The average superheat value at the interface is very small for the forth bubble, therefore the size of the forth bubble does not change much in the near wall region and gets smaller when it reaches the cooler liquid. The fluctuation in the bubble equivalent diameter reflects the bubble deformability while lifting off from the wall.

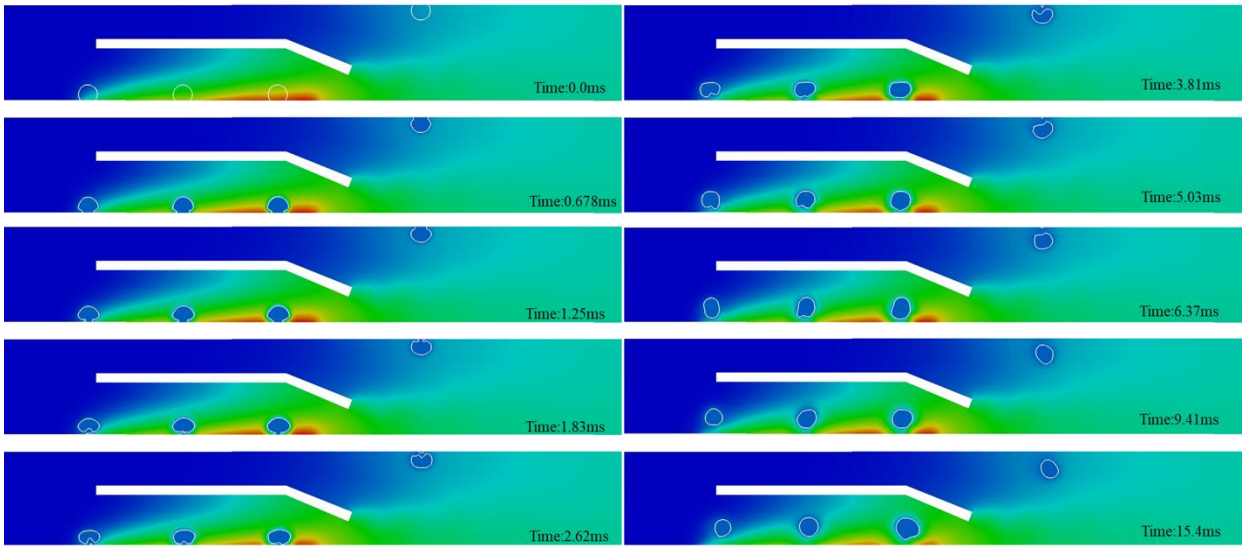

Figure 9. Bubble growth, departure and condensation evolution due to boiling phenomena over time based on the methodology developed in Li and Bolotnov[53].

The multiple bubble flow boiling scenario investigates the local bubble behavior in the unstructured mesh domain at four locations which exhibit qualitatively different behaviors. The bubble dynamics information is successfully collected for each bubble using BTA. The presented simulation demonstrates the boiling capabilities in the complex geometries when bubbles

differently react to local flow conditions. In the future, large scale simulations (Figure 3) will be performed utilizing the evaporation and condensation capabilities demonstrated here.

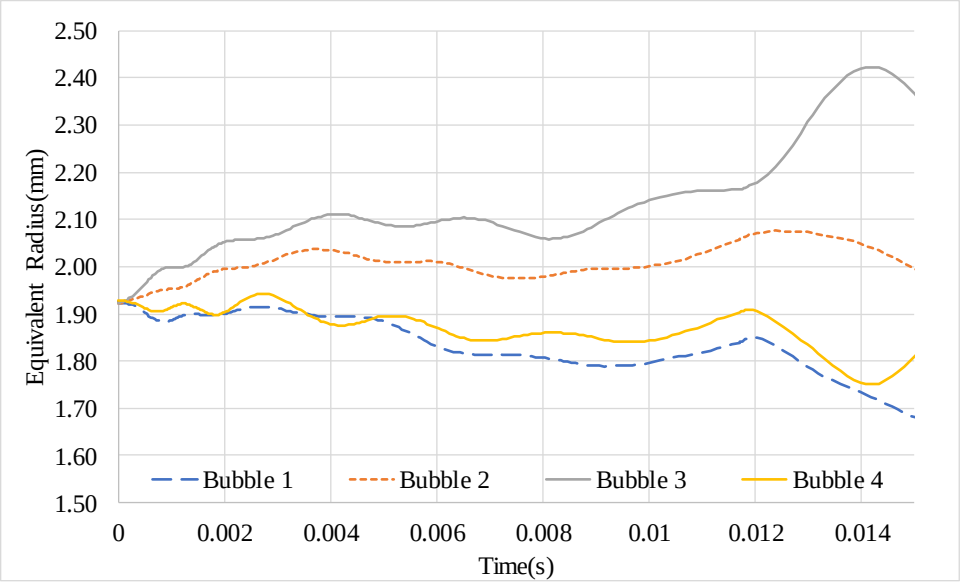

Figure 10. The growth rate of each bubble in flow boiling.

III.C. Dispersed flow film boiling (DFFB) simulations

During the reflood phase under the hypothetical loss-of-coolant accident (LOCA) in pressurized water reactors (PWRs), the dominant flow regime in the upper part of the reactor channels is the dispersed flow film boiling (DFFB). The DFFB regime is inherently transient, characterized by both mechanical and thermal non-equilibrium.[58,59] Phenomenologically speaking, it is best conceptualized by a mist type flow, with polydisperse droplets, corresponding to high void fractions (> 0.8).[60] Since the DFFB regime exists above the quench front, the dominant path of heat transfer under these conditions is to the entrained droplets. The major heat transfer mechanisms include radiation from the fuel rods to the droplets and vapor, convective heat transfer from the walls to the vapor, interfacial heat transfer from vapor to droplets and quenching of the rods due to droplet contact.[61] Another positive feedback to the overall heat transfer coefficient is

provided by droplet evaporation, resulting in steam de-superheating and vapor mass generation, enhancing convective heat transfer. It is evident that an accurate estimation of the droplet surface area is crucial to studying the heat transfer mechanisms. Thus, a detailed study of the droplet dynamics – its morphology, average diameter, interaction with surrounding flow, is indispensable to understanding the DFFB regime. Of particular interest is the droplet interaction with spacer-grid structures. Several prior experimental studies reported a sharp increase in heat transfer coefficient in the immediate downstream vicinity of spacer grid structures.[62–64] A stark observation from these experiments was the correlation of the increase in heat transfer to the increased surface area of droplets, post interaction with the spacer-grid structures. Cheung et al.[65] and Meholic et al.[66] have developed mechanistic heat transfer correlations to account for this phenomena.

DNS, coupled with the level-set interface tracking method, makes it feasible to study the droplet dynamics and its effects on the surrounding flow field upon interaction with the spacer-grid and mixing vane structures, under DFFB conditions. Herein we present two such high resolution adiabatic computational studies performed with and without the effect of gravity and qualitative discussion of the results obtained. Figure 11 shows an isometric view of the geometry used for both simulations, with the spacer-grid and mixing vane structures visible. This geometry is prototypal of commercial PWR reactors.

Table 3. Parameters for DFFB Simulations

Case	Re_g	ρ_{ratio}	μ_{ratio}	$u_d(m/s)$	We_c	We_a
RE1	5700	800	14	0.1	55	-
RE2_g	11,822	1000	48	2.05	55	0.319

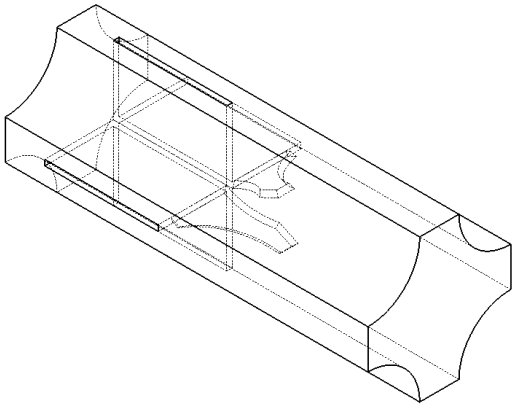

Figure 11. Subchannel with spacer grid and mixing vanes prototypal of commercial PWR reactors.

Table 3 enumerates the parameters selected for the simulations, including some important dimensionless numbers that are critical for characterizing two-phase flow dynamics. Most significantly, as is also reported by experimental observations by Cheung et al.[65], among others, the collision Weber number,

$$We_c = \frac{\rho_d D u_d^2}{\sigma} \tag{6}$$

where ρ_d is the droplet density, D is the droplet diameter, u_d is the absolute incident velocity of the droplet and σ is the surface tension force coefficient, is the critical parameter influencing droplet dynamics upon collision with spacer-grid structure. Spherical droplets are initialized at the upstream location of the spacer-grid, with a constant diameter of 1 mm for both simulations. The dimensionless numbers listed in Table 3 correspond to the state of the droplets at the point of inception. The aerodynamic Weber number is defined as,

$$We_a = \frac{\rho_g D u_{rel}^2}{\sigma} \tag{7}$$

where ρ_g is the gas phase density and u_{rel} is the relative velocity of the surrounding gas with respect to a droplet. It primarily characterizes the droplet behavior with respect to the surrounding

flow and is used to demarcate free stream breakup regimes.[67] Experiments of the DFFB regime indicate that after entrainment in the lower parts of the reactor channels, the small and large droplets roughly travel at the terminal velocity corresponding to the average droplet size, as observed near the spacer grids close to the peak power location.[58] Consistent with this observation the droplets are initialized for case RE2_g at the terminal velocity. The corresponding aerodynamic Weber for this velocity is 0.319, indicating that drag forces will have a negligible effect on droplet morphology. Note that for RE1 case the droplets are initialized, owing to the absence of gravity, with zero relative velocity with respect to the mean velocity of surrounding fluid. Thus, the aerodynamic Weber number, being negligible, is not listed. The droplet to gas density ratio and viscosity ratio correspond to a steam-water system at 40 psi (275,790 Pa) for the RE1 case and to air-water system at STP for the RE2_g case. The inlet gas Reynolds number is defined as,

$$Re_g = \frac{\rho_g D_h u_{mean}}{\mu_g} \tag{8}$$

where, D_h is the hydraulic diameter of the sub-channel at the inlet cross-section, u_{mean} is the mean velocity of the gas and μ_g is the gas dynamic viscosity. The selected value of Re_g for the RE1 case is similar to the steam Reynolds number reported by Riley et al. in their experiments.[62]

As mentioned earlier, increase in the surface area of droplets on collision with spacer-grids strongly correlates to the increase in heat transfer coefficient. Figure 12 shows the time evolution of morphology of droplets, as a result of intra droplet and droplet-structure interaction. The void fraction of the computational domain at t = 45.8 *ms* is 0.9492, which lies in the characteristic DFFB region. Also shown in the figure is the cross section of the domain 5*mm* from the incident surface of the spacer grid. The enclosed droplet area is demarcated from the gas by the solid black line. It is clearly evident that the droplets undergo significant deformation, resulting in an increase in their

surface area. An exact quantification of the time averaged surface area of droplets downstream of the spacer grids with respect to their upstream surface area remains in the immediate future scope of these simulations.

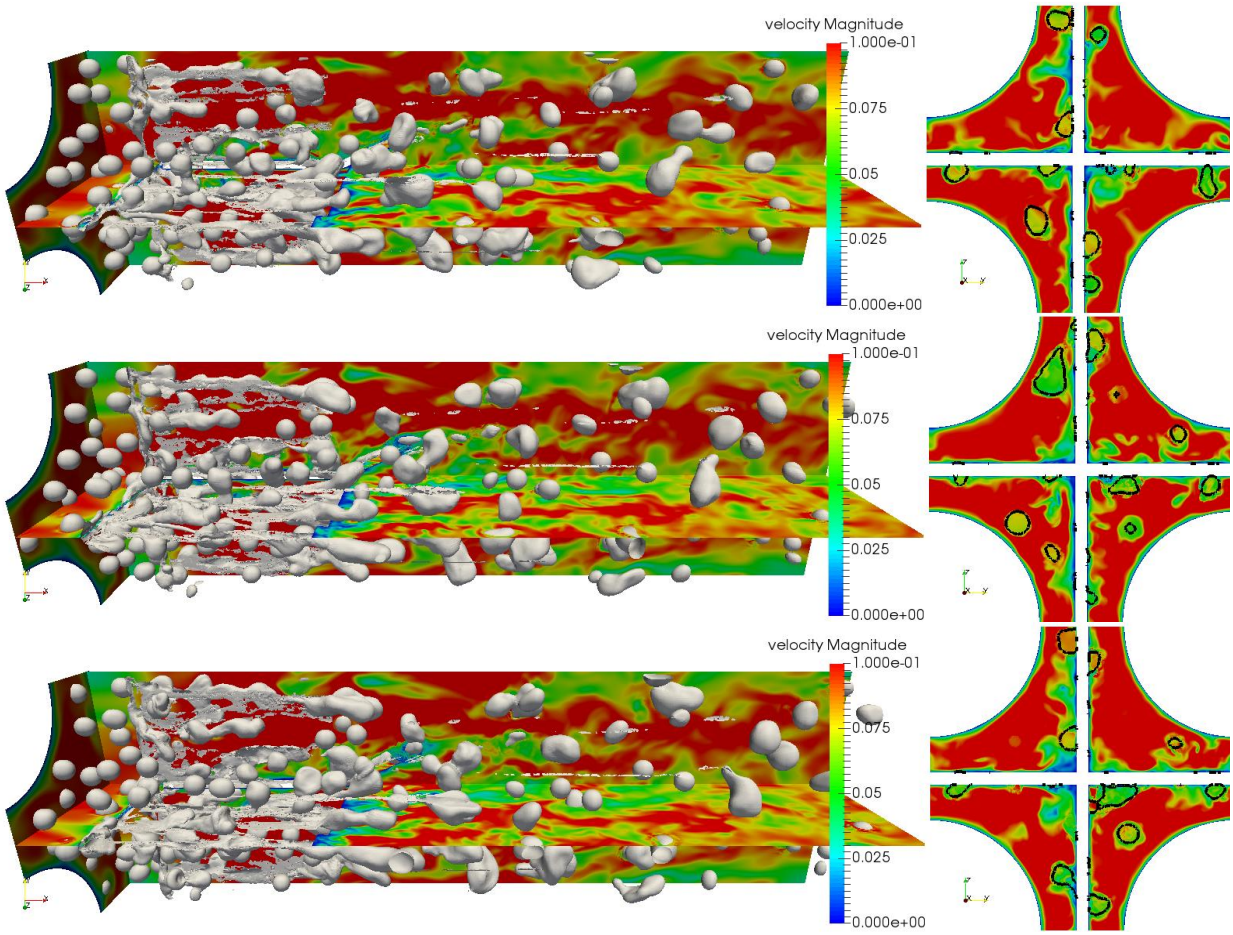

Figure 12. Droplet interaction with spacer-grid captured at t= 41.8, 43.8, and 45.8 ms for RE1 case.

It is interesting to note the differences in the post collision droplet behavior for the RE1 and RE2_g cases. For the latter case the droplet dynamics are governed not only by the drag and inertial forces, but also by gravitational force, which is absent for the former. Moreover, the magnitude of drag force in the RE2_g case is significantly higher, since the droplets are initialized with negligible relative velocity in the RE1 case. Further, upon collision there is an increase in the

relative ratio of surface area to volume, which directly correlates to the ratio of drag force to the body force, for the daughter droplets with respect to the parent droplet.

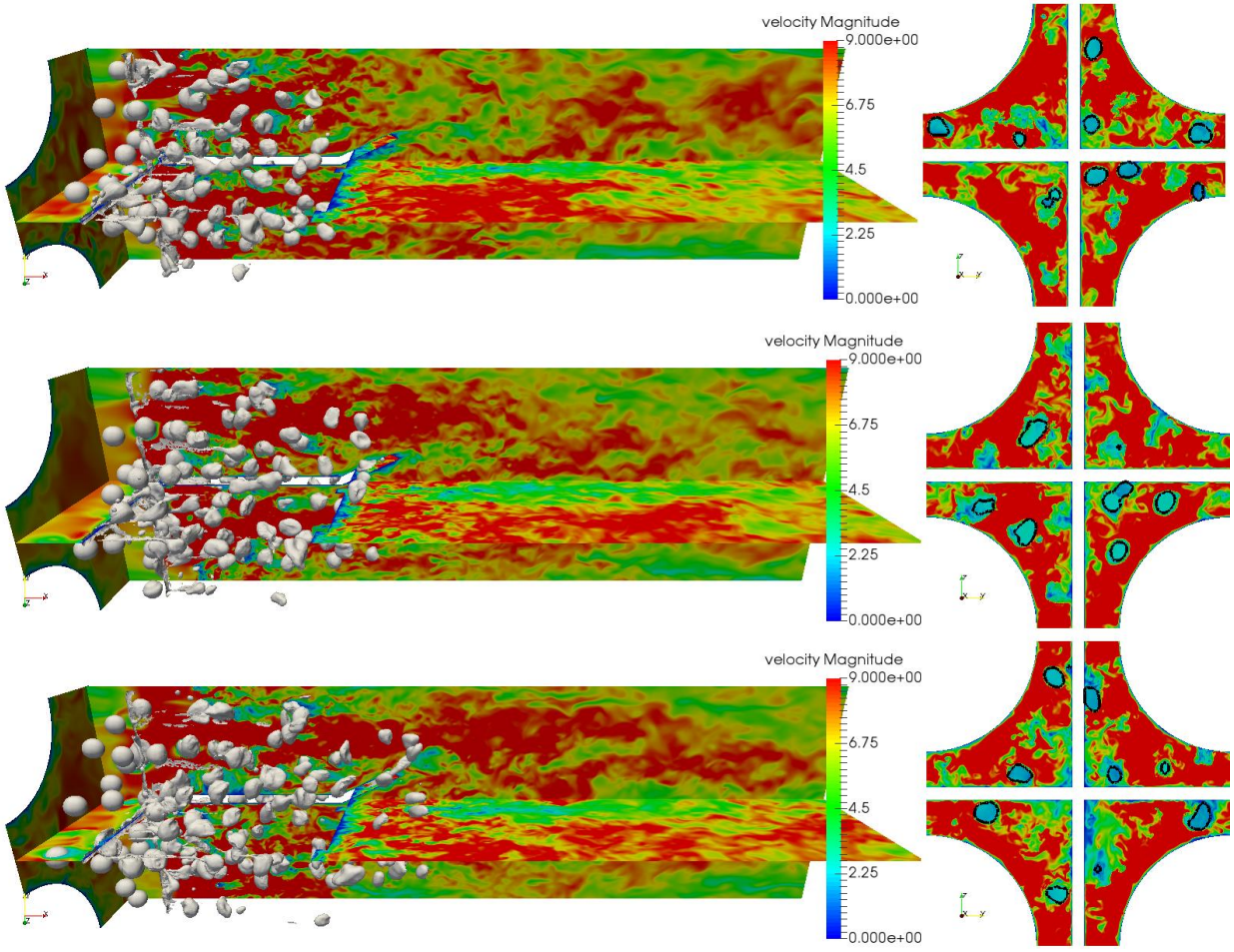

Figure 13. Droplet interaction with spacer-grid captured at t= 5.05, 6.05, and 7.05 ms for RE2_g case

$$\frac{F_d}{F_g} \sim \frac{surface\ area}{volume} \tag{9}$$

Consequently, the daughter droplets in the RE2_g case experience an acceleration in the streamwise direction. This can be seen manifested in Figure 13. The daughter droplets are less likely to coalesce with upstream droplets due to the effect of increased acceleration. In the previous case, however, the droplets retard due to collision with respect to the upstream, incoming droplets and thus they are more likely to merge into larger drops. Another stark difference in the droplet

behavior from the previous case is that they do not tend stick to the spacer-grid walls after collision. The daughter droplets retreat to the bulk flow, again, we surmise, due to the increase in relative drag force.

Thus, we demonstrate the capability of DNS and interface tracking method to model the complex intricacies of the DFFB regime. Further investigation is needed to provide a quantitative analysis of the simulations.

IV. CONCLUSIONS

In the presented paper we have discussed the progress of DNS-based simulations to advance the state-of-the-art thermal hydraulics models and perform high-resolution interface resolved simulations on very large scale. Several application examples are presented, including the bubbly flow simulation in PWR subchannel geometries, flow boiling simulation with multiple nucleation sites as well as the DFFB regime modeling with liquid droplets. These examples involve complex geometric structures, relatively higher Reynolds numbers, and even the phase change process, which clearly demonstrate the ever-closer engineering relevance to practical reactor thermal-hydraulics design problems. Future expansion of high-performance computing (such as the first U.S. exascale supercomputer, Aurora[68], expected in 2021) will allow to apply these complex simulations to realistic Reynolds number two-phase flows which may include thousands of bubbles boiling under nuclear reactor pressure/temperature conditions. Advanced data analysis techniques will allow to further improve existing models, such as the interfacial force closures or critical heat flux models, by mining the abundant numerical insights produced by these interface-resolved high-resolution simulations. The improved models will in turn benefit the lower-

resolution practical engineering predictions capable to resolve larger time transients and full reactor domains.

ACKNOWLEDGMENTS

The authors would like to acknowledge the support from the Consortium for Advanced Simulation of Light Water Reactors (CASL) (http://www.casl.gov). CASL is an Energy Innovation Hub for Modeling and Simulation of Nuclear Reactors under U.S. Department of Energy (DOE) [grant number DE-AC05-00OR22725] and by Department of Energy's Nuclear Energy University Program's Integrated Research Project "Development and Application of a Data-Driven Methodology for Validation of Risk-Informed Safety Margin Characterization Models". The lead author, Dr. Jun Fang, also would like to acknowledge his current employer Argonne National Laboratory for the support during the manuscript drafting and revising. Argonne is operated by UChicago Argonne, LLC, for the U.S. DOE under contract DE-AC02-06CH11357.

This research benefited from the computational resources provided by Argonne Leadership Computing Facility (ALCF), which is a DOE Office of Science User Facility supported under Contract DE-AC02-06CH11357 through computing hour awards of 2014, 2016 and 2018 ALCC programs. The solutions presented made use of software components provided by Altair Engineering (Acusim), Simmetrix (MeshSim and SimModeler), Kitware (ParaView).

REFERENCES

1. W. P. JONES and B. E. LAUNDER, "The prediction of laminarization with a two-equation model of turbulence," Int. J. Heat Mass Transf. **15** 2, 301, Pergamon (1972); https://doi.org/10.1016/0017-9310(72)90076-2.
2. B. E. LAUNDER and B. I. SHARMA, "Application of the energy-dissipation model of turbulence to the calculation of flow near a spinning disc," Lett. heat mass Transf. **1** 2, 131 (1974); https://doi.org/10.1016/0094-4548(74)90150-7.
3. B. E. LAUNDER and D. B. SPALDING, "Lectures in Mathematical Models of Turbulence," Acad. Press (1972); https://doi.org/10.1080/10256010903084126.
4. D. A. DREW and S. L. PASSMAN, *Theory of multicomponent fluids*, Springer Science & Business Media, New York (1998).
5. E. STROHMAIER et al., "The TOP500 List and Progress in High-Performance Computing," Comput. **48** 11, 42 (2015); https://doi.org/10.1109/MC.2015.338.
6. A. PROSPERETTI and G. TRYGGVASON, *Computational methods for multiphase flow*, Cambridge university press (2007).
7. I. A. BOLOTNOV et al., "Spectral analysis of turbulence based on the DNS of a channel flow," Comput. Fluids **39**, 640 (2010); https://doi.org/10.1016/j.compfluid.2009.11.001.
8. J. LU and G. TRYGGVASON, "Effect of bubble deformability in turbulent bubbly upflow in a vertical channel," Phys. Fluids **20** 4, 40701 (2008); https://doi.org/10.1063/1.2911034.
9. A. V. MISHRA and I. A. BOLOTNOV, "DNS of turbulent flow with hemispherical wall roughness," J. Turbul. **16** 3, 225 (2015); https://doi.org/10.1080/14685248.2014.989231.
10. R. D. MOSER, J. KIM, and N. N. MANSOUR, "Direct numerical simulation of turbulent channel flow up to Re=590," Phys. Fluids **11** 4, 943 (1999);

https://doi.org/10.1063/1.869966.

11. I. A. BOLOTNOV, “Influence of Bubbles on the Turbulence Anisotropy,” J. Fluids Eng. **135** 5, 051301, ASME (2013); https://doi.org/10.1115/1.4023651.
12. G. TRYGGVASON et al., “Multiscale considerations in direct numerical simulations of multiphase flows,” Phys. Fluids **25** 3, 31302, American Institute of Physics (2013); https://doi.org/10.1063/1.4793543.
13. S. B. POPE, *Turbulent flows*, Cambridge university press (2000).
14. D. C. WILCOX, *Turbulence Modeling for CFD*, DCW Industries (2002).
15. J. BOUSSINESQ, “Theorie de l’Ecoulement Tourbillant,” Mem.Presentes par Divers Savants Acad.Sci.Inst.Fr **23**, 46 (1877).
16. O. REYNOLDS, “On the dynamical theory of incmopressible viscous fluids and the determination of the criterion,” Philos. Trans. R. Soc. London **186** A, 123 (1895).
17. M. Z. PODOWSKI, “On the consistency of mechanistic multidimensional modeling of gas/liquid two-phase flows,” Nucl. Eng. Des. **239** 5, 933 (2009); https://doi.org/10.1016/j.nucengdes.2008.10.022.
18. M. ISHII and T. HIBIKI, *Thermo-fluid dynamics of two-phase flow*, Springer (2006).
19. R. T. LAHEY, “The simulation of multidimensional multiphase flows,” Nucl. Eng. Des. **235** 10–12 (2005); https://doi.org/10.1016/j.nucengdes.2005.02.020.
20. J. KIM, P. MOIN, and R. MOSER, “Turbulence statistics in fully developed channel flow at low Reynolds number,” J. Fluid Mech. **177**, 133 (1987); https://doi.org/10.1017/S0022112087000892.
21. M. LEE and R. D. MOSER, “Direct numerical simulation of turbulent channel flow up to Re_tau 5200,” J. Fluid Mech. **774**, 395 (2015); https://doi.org/10.1017/jfm.2015.268.

22. A. ASHRAFIAN, H. I. ANDERSSON, and M. MANHART, “DNS of turbulent flow in a rod-roughened channel,” Int. J. Heat Fluid Flow **25** 3 (2004); https://doi.org/10.1016/j.ijheatfluidflow.2004.02.004.

23. P. A. KROGSTAD et al., “An experimental and numerical study of channel flow with rough walls,” J. Fluid Mech. **530** (2005); https://doi.org/10.1017/S0022112005003824.

24. I. A. BOLOTNOV et al., “A spectral turbulent cascade model for single- and two-phase uniform shear flows,” J. Turbul. (2008); https://doi.org/10.1080/14685240802261102.

25. I. A. BOLOTNOV et al., “Spectral Cascade Modeling of Turbulent Flow in a Channel,” Japanese J. Multiph. Flow **23** 2, 190 (2009); https://doi.org/10.3811/jjmf.23.190.

26. R. SCARDOVELLI and S. ZALESKI, “Direct numerical simulation of free-surface and interfacial flow,” Annu. Mech. **31**, 567 (1999); https://doi.org/10.1146/annurev.fluid.31.1.567.

27. B. BUNNER and G. TRYGGVASON, “Effect of bubble deformation on the properties of bubbly flows,” J. Fluid Mech. **495**, 77 (2003); https://doi.org/10.1017/S0022112003006293.

28. M. SUSSMAN et al., “An improved level set method for incompressible two-phase flows,” Comput. Fluids **27** 5, 663 (1998); https://doi.org/10.1016/S0045-7930(97)00053-4.

29. M. ILIĆ, M. WÖRNER, and D. G. CACUCI, “Balance of Liquid-phase Turbulence Kinetic Energy Equation for Bubble-train Flow,” J. Nucl. Sci. Technol. **41** 3, 331, Taylor & Francis (2004); https://doi.org/10.1080/18811248.2004.9715492.

30. M. ILIĆ, M. WÖRNER, and D. G. CACUCI, “Evaluation of energy spectra in bubble driven liquid flows from direct numerical simulations,” in International conference on Multiphase Flow, July 9-13, 2007, Leipzig, Germany (2007).

31. J. LU, S. BISWAS, and G. TRYGGVASON, “A DNS study of laminar bubbly flows in a

vertical channel," Int. J. Multiph. Flow **32** 6, 643, Pergamon (2006); https://doi.org/10.1016/J.IJMULTIPHASEFLOW.2006.02.003.

32. G. BOIS, "Direct numerical simulation of a turbulent bubbly flow in a vertical channel: Towards an improved second-order reynolds stress model," Nucl. Eng. Des. **321**, 92, North-Holland (2017); https://doi.org/10.1016/J.NUCENGDES.2017.01.023.

33. A. DU CLUZEAU, G. BOIS, and A. TOUTANT, "Analysis and modelling of Reynolds stresses in turbulent bubbly up-flows from direct numerical simulations," J. Fluid Mech. **866**, 132, Cambridge University Press (2019); https://doi.org/10.1017/jfm.2019.100.

34. I. A. BOLOTNOV et al., "Detached direct numerical simulations of turbulent two-phase bubbly channel flow," Int. J. Multiph. Flow **37** 6, 647, Pergamon (2011); https://doi.org/10.1016/j.ijmultiphaseflow.2011.03.002.

35. S. ELGHOBASHI, "Direct Numerical Simulation of Turbulent Flows Laden with Droplets or Bubbles," Annu. Rev. Fluid Mech. **51** 1, 217, Annual Reviews (2019); https://doi.org/10.1146/annurev-fluid-010518-040401.

36. J. FANG, M. RASQUIN, and I. A. BOLOTNOV, "Interface tracking simulations of bubbly flows in PWR relevant geometries," Nucl. Eng. Des. **312** Supplement C, 205 (2017); https://doi.org/10.1016/j.nucengdes.2016.07.002.

37. J. FANG and I. A. BOLOTNOV, "Bubble tracking analysis of PWR two-phase flow simulations based on the level set method," Nucl. Eng. Des. **323** Supplement C, 68 (2017); https://doi.org/10.1016/j.nucengdes.2017.07.034.

38. J. FANG et al., "Direct numerical simulation of reactor two-phase flows enabled by high-performance computing," Nucl. Eng. Des. **330**, 409 (2018); https://doi.org/10.1016/j.nucengdes.2018.02.024.

39. J. FANG et al., “Interface Tracking Investigation of Geometric Effects on the Bubbly Flow in PWR Subchannels,” Nucl. Sci. Eng. **193** 1–2, 46 (2019); https://doi.org/10.1080/00295639.2018.1499280.

40. G. TRYGGVASON, A. ESMAEELI, and N. AL-RAWAHI, “Direct numerical simulations of flows with phase change,” Comput. Struct. (2005); https://doi.org/10.1016/j.compstruc.2004.05.021.

41. J. WU, V. K. DHIR, and J. QIAN, “Numerical simulation of subcooled nucleate boiling by coupling level-set method with moving-mesh method,” Numer. Heat Transf. Part B Fundam. **51** 6, 535 (2007); https://doi.org/10.1080/10407790601177763.

42. G. SON and V. K. DHIR, “Numerical simulation of nucleate boiling on a horizontal surface at high heat fluxes,” Int. J. Heat Mass Transf. **51** 9, 2566 (2008); https://doi.org/10.1016/j.ijheatmasstransfer.2007.07.046.

43. Y. OSE and T. KUNUGI, “Development of A Boiling and Condensation Model on Subcooled Boiling Phenomena,” Energy Procedia **9** 71, 605 (2011); https://doi.org/10.1016/j.egypro.2011.09.071.

44. S. NAGRATH et al., “Hydrodynamic simulation of air bubble implosion using a level set approach,” J. Comput. Phys. **215** 1, 98, Academic Press (2006); https://doi.org/10.1016/j.jcp.2005.10.020.

45. M. RASQUIN et al., “Scalable implicit flow solver for realistic wing simulations with flow control,” Comput. Sci. Eng. **16** 6, 13 (2014); https://doi.org/10.1109/MCSE.2014.75.

46. C. H. WHITING and K. E. JANSEN, “A stabilized finite element method for the incompressible Navier-Stokes equations using a hierarchical basis,” Int. J. Numer. Methods Fluids **35** 1, 93 (2001); https://doi.org/10.1002/1097-0363(20010115)35:1<93::AID-

FLD85>3.0.CO;2-G.

47. J. U. BRACKBILL, D. B. KOTHE, and C. ZEMACH, “A continuum method for modeling surface tension,” J. Comput. Phys. **100** 2, 335 (1992); https://doi.org/10.1016/0021-9991(92)90240-Y.

48. F. BEHAFARID, K. E. JANSEN, and M. Z. PODOWSKI, “A study on large bubble motion and liquid film in vertical pipes and inclined narrow channels,” Int. J. Multiph. Flow **75**, 288 (2015); https://doi.org/10.1016/j.ijmultiphaseflow.2015.04.016.

49. M. D. ZIMMER and I. A. BOLOTNOV, “Slug-to-churn vertical two-phase flow regime transition study using an interface tracking approach,” Int. J. Multiph. Flow **115**, 196, Pergamon (2019); https://doi.org/10.1016/J.IJMULTIPHASEFLOW.2019.04.003.

50. J. RODRIGUEZ et al., “A parallel adaptive mesh method for the numerical simulation of multiphase flows,” Comput. Fluids **87**, 115 (2013); https://doi.org/10.1016/j.compfluid.2013.04.004.

51. M. LI, “High Resolution Boiling Simulation Using Interface Tracking Method,” North Carolina State University (2019).

52. M. LI and I. A. BOLOTNOV, “The Evaporation and Condensation Model with Interface Tracking,” Int. J. Heat Mass Transf. **Submitted** (2019).

53. M. LI and I. A. BOLOTNOV, “Interface Tracking Simulation of Phase-Change Phenomena: Boiling and Condensation Verification,” in ASME 2016 Summer Conference, p. V01AT06A001, Washington, DC (2016); https://doi.org/10.1115/FEDSM2016-7701.

54. M. LI et al., “Development of a New Contact Angle Control Algorithm for Level-Set Method,” J. Fluids Eng. **141** 6, 61301, ASME (2018); https://doi.org/10.1115/1.4041987.

55. Y. SATO and B. NICENO, “A depletable micro-layer model for nucleate pool boiling,” J.

Comput. Phys. **300**, 20 (2015); https://doi.org/10.1016/j.jcp.2015.07.046.

56. J. KIM, "Review of nucleate pool boiling bubble heat transfer mechanisms," Int. J. Multiph. Flow **35** 12, 1067 (2009); https://doi.org/10.1016/j.ijmultiphaseflow.2009.07.008.

57. M. LI and I. A. BOLOTNOV, "Development of Evaporation and Condensation Model – Pool Boiling Simulation using ITM approach," in 2018 ANS Annual Meeting, Philadelpiha, PA (2018).

58. K. H. ARDRON and P. C. HALL, "Droplet hydrodynamics and heat transfer in the dispersed flow regime in bottom flooding," Berkeley (1981).

59. N. LEE et al., "PWR FLECHT SEASET unblocked bundle, forced and gravity reflood task. Data evaluation and analysis report," United States Regulatory Commission, Washington, DC (1982).

60. M. ANDREANI and G. YADIGAROGLU, "Dispersed flow film boiling (PSI--51)," Switzerland (1989).

61. M. ANDREANI and G. YADIGAROGLU, "Prediction methods for dispersed flow film boiling," Int. J. Multiph. Flow **20**, 1, Pergamon (1994); https://doi.org/10.1016/0301-9322(94)90069-8.

62. M. P. RILEY et al., "Experimental Studies of Spacer Grid Thermal Hydraulics in the Dispersed Flow Film Boiling Regime," Nucl. Technol. **190** 3, 336 (2015); https://doi.org/10.13182/NT14-80.

63. D. J. MILLER, F. B. CHEUNG, and S. M. BAJOREK, "Investigation of grid-enhanced two-phase convective heat transfer in the dispersed flow film boiling regime," Nucl. Eng. Des. **265**, 35, North-Holland (2013); https://doi.org/10.1016/J.NUCENGDES.2013.07.013.

64. S. C. YAO, L. E. HOCHREITER, and W. J. LEECH, "Heat-Transfer Augmentation in Rod

Bundles Near Grid Spacers," J. Heat Transfer **104** 1, 76, ASME (1982); https://doi.org/10.1115/1.3245071.

65. F. B. CHEUNG and S. M. BAJOREK, "Dynamics of droplet breakup through a grid spacer in a rod bundle," Nucl. Eng. Des. **241** 1, 236, North-Holland (2011); https://doi.org/10.1016/J.NUCENGDES.2010.10.017.

66. M. J. MEHOLIC, D. L. AUMILLER, and F.-B. CHEUNG, "A comprehensive, mechanistic heat transfer modeling package for dispersed flow film boiling – Part 1 – Development," Nucl. Eng. Des. **291**, 295, North-Holland (2015); https://doi.org/10.1016/J.NUCENGDES.2015.07.013.

67. A. WIERZBA, "Deformation and breakup of liquid drops in a gas stream at nearly critical Weber numbers," Exp. Fluids **9** 1, 59 (1990); https://doi.org/10.1007/BF00575336.

68. ANL, "Aurora, coming in 2021;" 2019; https://press3.mcs.anl.gov/aurora/; (current as of Apr. 15, 2019).